Evolution of the Image Quality over Time for a Freehand Monostatic mm-Wave Radar Imager

Guillermo Álvarez-Narciandi*, Jaime Laviada*, Fernando Las-Heras*
*Dept. of Electrical Engineering, University of Oviedo, Gijón, Spain, alvareznguillermo@uniovi.es

***Abstract*—In this paper the performance over time of a freehand, mm-wave imaging scanner is studied. The system comprises a FMCW on-chip-radar and a motion capture system used to estimate the position of the scanner during the acquisition process in order to coherently combine the measured data creating a synthetic aperture. The scanner is controlled by a conventional laptop, which is also in charge of processing the obtained data displaying real-time results. Specifically, four snapshots (i.e., intermediate results) of the same scan comprising a target hidden under a hard cardboard box are analyzed. The obtained results show that only a few seconds can be enough to retrieve a rough estimation of the shape of the targets within the volume under test.**

***Index Terms*—Freehand imaging, SAR imaging, mm-wave imaging, FMCW radar, real-time imaging.**

I. Introduction

Electromagnetic imaging systems can build the image of an object by measuring its scattered field. Particularly, mm-waves provide a good trade-off between resolution and penetration capabilities for a large number of applications. The development of mm-wave scanners for security applications [1], non-destructive evaluation (NDE) [2] and industrial applications [3] has been a hot research topic. Most of the aforementioned scanners are based on moving along a two dimensional plane an array of transceivers to create synthetic apertures, improving the cross-range resolution. Alternatively, other scanners comprise hundreds of transceivers to build a real aperture taking advantage of the high level of integration of mm-wave technology recently achieved [4]. A hybrid approach has been proposed by means of portable scanners exploiting multiview information (resembling computer vision techniques), which can be manually moved in order to obtain multiple views of the volume under test [5], [6], [7]. Recently, a freehand scanner based on a mm-wave frequency modulated continuous wave (FMCW) radar with a monostatic configuration has been proposed [8]. The system, which is cost-effective and compact, exploits the freehand movements of the scanner to create a synthetic aperture. In particular, the system employs a time-domain backprojection algorithm [9] to obtain real-time reflectivity images of the volume under scan so that the operator can determine if any part of it needs to be further inspected. In this paper, the quality of the obtained results versus acquisition time, i.e., the number of radar acquisitions, is analyzed comparing the reflectivity image obtained at several snapshots during a scan of a test target.

II. System Architecture

First, the architecture of the imaging system proposed in [8], based on a mm-wave FMCW radar, is briefly reviewed. The radar is freely moved over the volume under test (Fig. 1), which imposes several constraints to each component of the system. In particular, the scanner must be lightweight and compact and the accuracy provided by the positioning subsystem should be high enough (errors below $\lambda/10$ at mm-wave frequencies) in order to coherently combine the radar measurements. In addition, the signal processing performed to obtain reflectivity images must ensure real-time operation without requiring a regular spatial sampling.

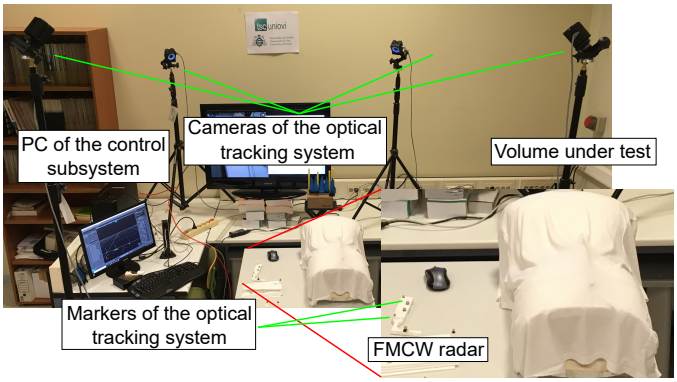

Fig. 1. Setup of the proposed system.

The system is structured in the three subsystems described below:

- Control and processing subsystem: queries the radar frames comprising IF data and its position to the other subsystems and processes the received data to obtain real-time images of the volume under scan. This subsystem is composed of a PC, which is connected with the radar subsystem by a USB port and with the positioning subsystem by an Ethernet connection (Fig. 2).
- Radar subsystem: transmits and receives the radar signals when required by the control subsystem and sends the IF signal to the Control and processing subsystem for further processing. This subsystem is composed of the BGT60TR24B radar transceiver (Fig. 3) of Infineon® [10], which includes the RF frontend and the USB interface that makes possible to send the IF signal to the control PC. The waveform of the signal transmitted by the radar has an up-chirp saw tooth pattern. The central

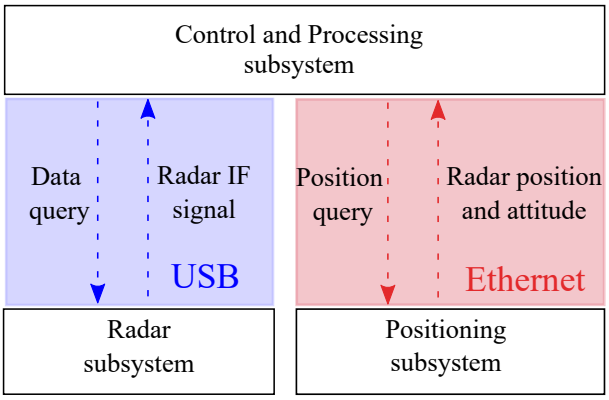

Fig. 2. Block diagram and information flow of the proposed system.

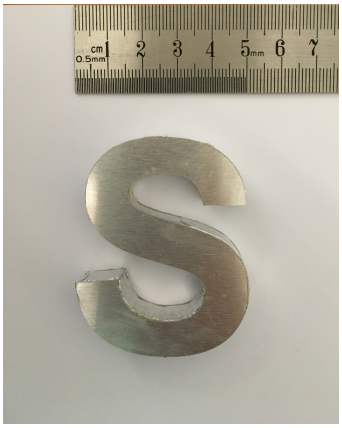

Fig. 4. Scanned target.

frequency of the radar is $f_c = 60\,\text{GHz}$, the bandwidth was set to $BW = 6\,\text{GHz}$ and the chirp duration, i.e., the duration of the frequency ramp of the radar signal, to $T_s = 512\,\mu\text{s}$. The RF frontend includes 2 transmitting and 4 receiving low directivity patch antennas. However, for this system a *quasimonostatic* configuration with one transmitting and one receiving antenna was considered.

- Positioning subsystem: estimates the position and the attitude of the radar by means of an optical tracking system. This subsystem is formed by the motion capture system of Optitrack® [11]. The cameras of the system (Fig. 1) track the markers attached to the radar module. The position retrieved by the positioning system, which is the centroid of the deployed markers, must be translated to match the position of the radar.

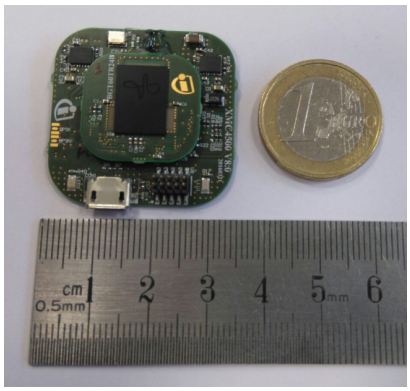

Fig. 3. FMCW radar module used for the imaging system.

III. Methodology

During the data acquisition, the radar is freely moved over the volume under test. However, in order to avoid high reflectivity areas due to an imbalance on the sample distribution, i.e., some areas concentrate a large number of samples with respect to other undersampled areas, a virtual reference plane over the volume under test is defined. This reference plane is discretized in a grid of cells within which only a maximum number of samples is allowed. In addition, to limit the impact of scanning along a non-flat surface, a tolerance value with respect to the reference plane is defined so that only measurements within that tolerance are considered valid.

The reflectivity of the volume under test is updated after performing a set of P radar and position acquisitions. In particular, both the radar IF signal and its position are queried and buffered until a set of three acquisitions is made in order to improve the real-time performance of the system. The delay and sum algorithm used to update the reflectivity of the volume under test is briefly reviewed below. The signal transmitted by the radar, expressed in complex form, is given by

$$s_{tx}(t) = e^{j2\pi(f_c t + \frac{1}{2}\alpha t^2)}, \tag{1}$$

where $|t| < T_s/2$ and

$$\alpha = \frac{BW}{T_s}, \tag{2}$$

is the slope rate. If a point target is considered, the signal received by the radar, omitting amplitude variations, can be expressed as a delayed version of the transmitted signal

$$s_{rx}(t) = s_{tx}(t-\tau) = e^{j2\pi(f_c(t-\tau)+\frac{1}{2}\alpha(t-\tau)^2)}, \tag{3}$$

where the delay τ, which is proportional to the distance from the radar position to the point target, R, is given by

$$\tau = \frac{2R}{c}. \tag{4}$$

The radar module used in this work performs dechirp-on-receive operations, i.e, the received and transmitted signals are mixed [12][13]. Therefore, the IF analytical signal, which is processed to estimate the reflectivity of the volume under test, can be expressed as

$$s_{IF}(t) = e^{j2\pi(f_c\tau + \alpha t\tau - \frac{1}{2}\alpha\tau^2)}, \tag{5}$$

which has beat frequency $f_b = \tau\alpha$. If the object under test is a distributed target, the received signal can be expressed as a

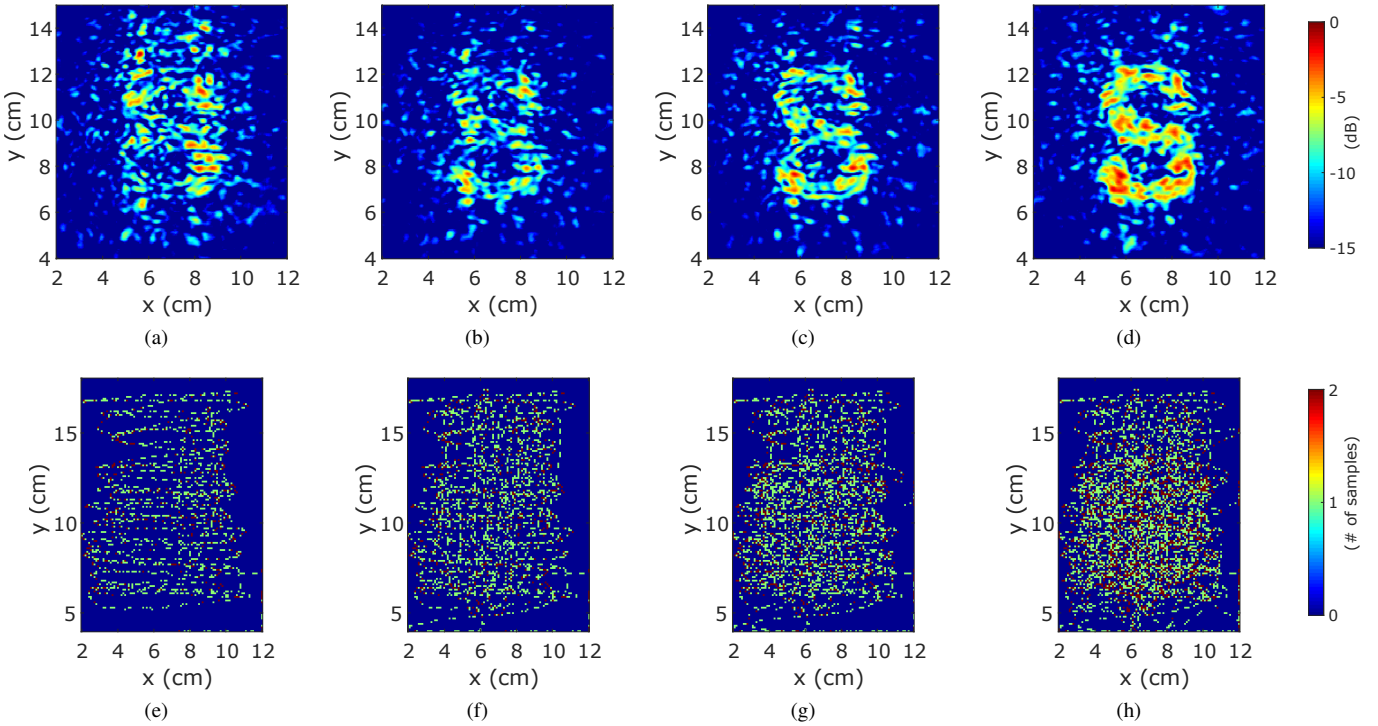

Fig. 5. Estimated reflectivity in one of the planes of the volume under test after 2015 samples were acquired (a) and the heat map showing their positions (e). The same information is presented for a snapshot of the scan after 3171 acquisitions, (b) and (f), respectively; after 4188 samples, (c) and (g), respectively; and after 6221 acquisitions, respectively.

superposition of signals given by (3), and the same holds for the IF signal.

The reflectivity at each point of the grid in which the volume under test is discretized is estimated by coherently combining the contribution of the signal received by the radar at each acquisition position by means of a time domain backprojection algorithm [9]. In order to do so, the signal acquired at the radar m-th radar position is multiplied by a complex exponential term that accounts for the theoretical delay between the radar position and each point of the volume under test. This signal is given by

$$s(t,m) = e^{-j2\pi f_c \tau_m} = e^{-j\frac{4\pi}{c} f_c R_m}, \tag{6}$$

where

$$R_m = \sqrt{(x'-x)^2 + (y'-y)^2 + (z'-z)^2}, \tag{7}$$

is the euclidean distance between the m-th radar position and each point of the volume under test, denoted by primed coordinates. Therefore, using this algorithm, the reflectivity image is updated in real-time after each set of acquisitions of the radar. It should be noticed that there are several methods that can be applied to coherently combine the measurements in real-time. However, most of them are based on Fast Fourier Transforms and thus, they require uniform sampling [14].

IV. Results

The performance of the system over time of the system was tested by scanning the target depicted in Fig. 4 covered by a hard-cardboard box. In this case, the size of the cells used to control the sample distribution was set to 1×1 mm and a tolerance of 2 cm was defined to mitigate the impact of not constraining the scan to a flat surface while allowing the operator to move comfortably the scanner with their hand over the volume under test. The mean distance from the scanner to the target was 6.1 cm and the maximum number of acquisitions per cell was set to 2. The obtained results for four different snapshots during a scan are depicted from Fig. 5a to Fig. 5d.

The reflectivity image displayed in Fig. 5a was obtained after 92 s and a total of 2105 samples. The heat map, depicting the positions at which acquisitions were made, is shown in Fig. 5e. As it can be observed, a high reflectivity area appears on the center of the image, although the shape of the target cannot be recognized as many image artifacts are present. It should be pointed out that, at that snapshot, there are some undersampled areas in the center of the volume under test that contribute to make the image noisier.

The results obtained at the second snapshot of the scan (after 153 s) are shown in Fig. 5b. The heat map depicting the positions of the 3171 acquisitions is displayed in Fig. 5f. In this case, the shape of the target can be inferred, although the magnitude of the reflectivity is not very high, being comparable to that of some of the image artifacts.

The reflectivity image retrieved after 200 s and a total of 4188 samples is depicted in Fig. 5c and the heat map showing the sample distribution is displayed in Fig. 5g. As it can be seen, the contrast between the target and the background has been enhanced with respect to the reflectivity image corresponding to the second snapshot (Fig. 5b). Although, there are some high reflectivity areas between the beginning

and the end of the S-shaped target and its center body, which could be interpreted as an "8" instead of as an "S", the quality of the obtained image is good.

Finally, the results obtained after completing the scan, after 6221 acquisitions and 301 s, are depicted in Fig. 5d. The heat map with the final sample distribution is illustrated in Fig. 5h. As it can be observed, the shape of the target is well-reconstructed and can be clearly distinguished from image artifacts.

V. Conclusion

In this paper the evolution of the quality over time of the reflectivity images obtained using the mm-wave radar-based handheld imaging system presented in [8] has been assessed. First, the architecture of the system, which comprises a mm-wave radar-on-chip module, a motion capture system and a conventional laptop to process the acquired data in real-time, and the employed imaging technique have been briefly reviewed. Then, the performance of the system over time was analyzed by comparing four snapshots during a scan of a target hidden under a hard cardboard box. The obtained results show that a scan of a few seconds can be enough to retrieve a rough estimation of the shape of the targets within the volume under test. In addition, if more data is acquired high quality images can be obtained. Future work involves the development of a MIMO configuration to speed up the data acquisition and, hence, reducing the time required to obtain high-resolution images.

Acknowledgment

This work has been supported by the Ministerio de Educación y Formación Profesional of Spain under the FPU grant FPU15/06431, by the Ministerio de Ciencia, Innovación y Universidades under project RTI2018-095825-B-I00 and by the Principado de Asturias/FEDER under project IDI/2018/000191.

References

[1] D. M. Sheen, D. L. McMakin, and T. E. Hall, "Three-dimensional millimeter-wave imaging for concealed weapon detection," *IEEE Transactions on Microwave Theory and Techniques*, vol. 49, no. 9, pp. 1581–1592, Sep 2001.

[2] S. Kharkovsky, J. T. Case, M. A. Abou-Khousa, R. Zoughi, and F. L. Hepburn, "Millimeter-wave detection of localized anomalies in the space shuttle external fuel tank insulating foam," *IEEE Transactions on Instrumentation and Measurement*, vol. 55, no. 4, pp. 1250–1257, Aug 2006.

[3] M. Vogt, M. Gerding, and T. Musch, "Implementation and evaluation of coherent synthetic aperture radar processing for level measurements of bulk goods with an fmcw-system," in *URSI Landesausschuss in der Bundesrepublik Deutschland*, Oct 2009, pp. 7–11.

[4] S. S. Ahmed, A. Schiessl, and L. P. Schmidt, "A novel fully electronic active real-time imager based on a planar multistatic sparse array," *IEEE Transactions on Microwave Theory and Techniques*, vol. 59, no. 12, pp. 3567–3576, Dec 2011.

[5] J. Laviada, A. Arboleya-Arboleya, Y. Alvarez, B. Gonzalez-Valdes, and F. Las-Heras, "Multiview three-dimensional reconstruction by millimetre-wave portable camera," *Sci. Rep.*, vol. 7, Jul 2017.

[6] J. Laviada, A. Arboleya-Arboleya, and F. Las-Heras, "Multistatic millimeter-wave imaging by multiview portable camera," *IEEE Access*, vol. 5, pp. 19 259–19 268, 2017.

[7] M. T. Ghasr, M. A. Abou-Khousa, S. Kharkovsky, R. Zoughi, and D. Pommerenke, "Portable real-time microwave camera at 24 ghz," *IEEE Transactions on Antennas and Propagation*, vol. 60, no. 2, pp. 1114–1125, Feb 2012.

[8] G. Álvarez-Narciandi, M. López-Portugués, F. Las-Heras, and J. Laviada, "Freehand, agile, and high-resolution imaging with compact mm-wave radar," *IEEE Access*, vol. 7, pp. 95 516–95 526, 2019.

[9] A. Ribalta, "Time-domain reconstruction algorithms for fmcw-sar," *IEEE Geoscience and Remote Sensing Letters*, vol. 8, no. 3, pp. 396–400, May 2011.

[10] I. Nasr, R. Jungmaier, A. Baheti, D. Noppeney, J. S. Bal, M. Wojnowski, E. Karagozler, H. Raja, J. Lien, I. Poupyrev, and S. Trotta, "A highly integrated 60 ghz 6-channel transceiver with antenna in package for smart sensing and short-range communications," *IEEE Journal of Solid-State Circuits*, vol. 51, no. 9, pp. 2066–2076, Sept 2016.

[11] OptiTrack. (2018, Feb.) Optitrack motion capture system. [Online]. Available: http://www.optitrack.com

[12] A. Meta, P. Hoogeboom, and L. P. Ligthart, "Signal processing for fmcw sar," *IEEE Transactions on Geoscience and Remote Sensing*, vol. 45, no. 11, pp. 3519–3532, Nov 2007.

[13] J. Barowski, I. Rolfes, and C. Baer, "Real-time imaging system for millimeter wave synthetic aperture radar sensors," in *2017 First IEEE MTT-S International Microwave Bio Conference (IMBIOC)*, May 2017, pp. 1–3.

[14] J. Yang, J. Thompson, X. Huang, T. Jin, and Z. Zhou, "Fmcw radar near field three-dimensional imaging," in *2012 IEEE International Conference on Communications (ICC)*, June 2012, pp. 6353–6356.